Magnetic Ultrathin Tissue Sections for Ease of Light and Electron Microscopy

G. Köstinger[1], D. Düring[1], S. Rickauer[1], V. Leite[1], H. Yamahachi[1], G. Csucs[2], R.H.R. Hahnloser[1,3*]

[1]Institute of Neuroinformatics, University of Zurich and ETH Zurich, Winterthurerstrasse 190, 8057 Zurich, Switzerland

[2]Scientific Center for Optical and Electron Microscopy (ScopeM), ETH-Zürich, 8093 Zürich, Switzerland

[3]Neuroscience Center Zurich, University of Zurich and ETH Zurich, 8057 Switzerland.

[*]rich@ini.ethz.ch

Abstract

Electron microscopy (EM) tends to be a tedious imaging technique that requires a diverse manual skill set, in particular when it comes to collecting and processing large numbers of consecutive ultrathin sections of biological tissue. To alleviate the challenges of collecting freshly cut sections floating on the water surface of an ultramicrotome, resins can be enhanced with nanoparticles to allow for accumulation of ultrathin sections under a magnet. Subsequent water removal deposits the dense section conglomerate onto an immersed EM imaging substrate. We describe an application of this workflow, termed Magnetic Section Collection (MagC), on ultrathin sections that were deposited on a silicon wafer and imaged in both light and scanning electron microscopes. We show that fluorescence data from three types of retrograde neuronal tracers are highly informative about projection neuron type and we propose a simple approach for neuron identification based on counting the percentage of consistently colored pixels across adjacent ultrathin sections.

Introduction

Electron microscopy (EM) has undergone a small revolution since the advent of digital imaging. Digitalization has brought convenience and high-throughput to otherwise labor-intense imaging workflows [1, 2]. However, many EM techniques remain labor intense, because they rely on ultramicrotomy, whereby a resin-embedded block of biological tissue is cut into consecutive sections, each only several tens of nanometers thick. Typically, after cutting, ultrathin sections float on the water surface of the knife boat and must be manually collected and placed on an imaging substrate. Both these tasks are prone to handling errors.

Recent advances have brought automation to the section collection process. In Automated Tape Collection Ultramicrotomy (ATUM) [3], ultrathin sections are first collected on a tape and then imaged in a Scanning Electron Microscope (SEM). Although the ATUM approach can provide non-destructive random access to an orderly collection of ultrathin sections, it entails several inconveniences: First, the tape needs further handling before imaging. Second, the collection substrate, a carbon-coated Kapton tape, emits auto-fluorescence, which hinders light-microscopy (LM) and along with it applications in array tomography (AT), whereby large numbers of ultrathin sections are histochemically processed and imaged in a light microscope [4]. Third, the accumulated tissue sections end up packed at a low density on the final imaging substrate, which can increase the cost of chemical post-processing and, in case of large volumetric requirements, may entail more frequent loading and unloading of the EM imaging chamber.

Recently, a new technique, termed Magnetic Section Collection (MagC) was developed that minimizes handling of ultrathin tissue sections and that is highly suited for post-embedding tissue processing [5, 6]. MagC takes advantage of superparamagnetic nanoparticles to make ultrathin tissue samples responsive to magnetic fields. Upon cutting, the magnetic sections can be densely grouped on the water surface using a magnet. The magnet maintains a high packing density of sections while they are deposited on an imaging substrate such as a silicon wafer. A relatively large MagC dataset in Correlative Array Tomography (CAT) [7] has recently been presented [6]. We inspect this dataset for consistent coloring across consecutive sections and propose a simple method for projection neuron identification.

Materials and Methods

All materials were acquired at Sigma-Aldrich Chemie GmbH, unless noted otherwise.

Magnetic resin

We prepared magnetic resin with 8% w/w of iron oxide superparamagnetic nanoparticles (CANdots M 4 nm Center for Applied Nanotechnology Hamburg, Germany, #SMB-0-039) in 1 g DGBA epoxy resin (Diglycidylether of Bisphenol A, # D3415 Sigma Aldrich; note: Bisphenol A monomer is widely used for manufacturing plastics and epoxies). The DGBA resin was stirred with a glass stirring staff in a watch glass on a heating plate at 90°C. After several minutes, when the heated resin was in a homogeneous state, 800 µl CAN DotSeries M org. SMB0-039 were added, followed by

stirring until the mixture appeared homogeneous. The mixture was then covered and cooled down to room temperature to keep the resin components from separating. At room temperature, 60 µl N, N- Dimethylbenzylamine, # Sigma 185582 (BDMA) and 5 µl Durcupan ACM single component D (# 44614 Sigma) were added one by one to the mixture under a hood. Thereafter, the resin mixture was slowly heated to 90°C (to prevent it from getting heterogeneous), whilst stirring for 15 - 20 minutes. While still hot, the mixture was placed on Aclar embedding Film (# TED PELLA, INC.) and was coated with mold separating agent (Glorex, # Antiglomerate Glorex.com Art 62407445) using a soft brush. Afterwards, the final resin mixture was cured overnight in an oven at 70°C. In case of inhomogeneous resin hardening, a properly hardened resin piece was selected for further processing.

Unlike in [6], the resin-embedded tissue was glued onto the magnetic resin with cyanoacrylate adhesive and trimmed with a razor blade, followed by trimming with a diamond knife (Trimtool 20, Diatome US).

Sectioning and collection

For ultrathin sectioning, a diamond knife was mounted with a clearance angle of 35 degrees on a custom-built bath of dimensions 55 x 44 mm^2 (now available as Ultra ATS, Diatome [8]). The bath was attached to an ultramicrotome (EM UC6, Leica). To manipulate the sections, a cylindrical neodymium magnet (15 mm diameter, 8 mm height, Supermagnete) was mounted facing down on a 3-axis motorized actuator (LTS150/M and PT1/M-Z8, Thorlabs) carrying a goniometer (GN2/M, Thorlabs). Using the goniometer, the orientation of the magnet was adjusted to make its face parallel to the water surface.

As the collection substrate, a silicon wafer of 2 cm x 2 cm was used. To make the surface hydrophilic, the wafer was treated with oxygen plasma for 1 minute with a coating current of 25 mA (K100X, Emitech). The substrate was laid onto three coverslips at the bottom of the boat at an angle of approximately 2 degrees. This tilt ensured that the water did not collect in the middle of the substrate during draining. The knife boat was filled with double distilled water using a 50 ml syringe mounted on a syringe pump (KDS 210, KD Scientific Inc.). The water was delivered and drained through a hole at the bottom of the boat.

Initially, a few sections were cut with the custom large knife to ensure proper alignment of the diamond with the block. Thereafter, 50 nm-thick sections were cut at a speed of

0.4 mm/s and collected on the water surface. During sectioning, an antistatic device (EM Crion, Leica) was placed about 2 to 8 cm away from the knife edge and turned on at maximal power.

After sectioning, the magnet was lowered to about 1 mm above the water surface. Using a custom script, the magnet scanned the water surface at a speed of about 1 mm/s in order to collect and assemble all the sections in the center of the bath. Sections that had been stuck at the wall of the boat were released using an eyelash. To deposit the sections on the silicon wafer, the water was slowly removed with the syringe pump (rate 5 ml/min). The magnet's position was semi-automatically maintained at about 1 mm above the water level. Upon water removal, a heating pad warmed the knife boat to about 40 °C to speed up evaporation, before placing the substrate for 30 minutes on a hot plate at 50 °C.

CAT dataset

We analyzed a CAT dataset [6] in which neural tracers were injection into diverse brain areas as follows:

1) Alexa Fluor 488 into the robust nucleus of the arcopallium (RA).
2) Fluorescein into Area X.
3) Texas Red into Avalanche.

Immunohistochemical processing was performed in a first step using

1) rat anti-Alexa Fluor 488,
2) mouse anti-fluorescein, and
3) goat anti-rhodamine.

In a second step, the sections were treated for 1 h with a secondary antibody in a 1:100 dilution in blocking solution:

1) Alexa Fluor 488 Donkey anti-rat,
2) Alexa fluor 647 donkey anti-mouse, and
3) Alexa Fluor 546 rabbit anti-goat.

Details of the correlative imaging procedure are provided at [6] and https://doi.org/10.3929/ethz-b-000267370.

LM analysis

The 3d positions of the 7 analyzed neurons are as follows.

#1: 27707, 22114, 58: http link 1
#2: 14281, 10914, 375: http link 2
#3: 6779, 13023, 71: http link 3
#4: 25137, 16549, 274 : http link 4
#5: 14557, 8699, 500 : http link 5
#6: 24716, 10672, 165 : http link 6
#7: 23649, 10862, 399 : http link 7

To inspect these neurons, please visit https://goo.gl/S9pduA, where the CAT data from 512 sections (corresponding to a brain volume of 300 µm x 200 µm x 25 µm) are posted. Online visualization is provided with Neurodataviz [16], an instance of Neuroglancer [17], hosted online. The 680 GB dataset will be hosted there for two years, thereafter, we provide access upon request.

Results

Manipulation of magnetically augmented ultrathin sections

The idea behind MagC is to magnetically augment the resin in which the tissue sample is embedded by coupling it to a piece of magnetic resin. To independently verify an initial report on using MagC [6], we produced magnetic resin by heating standard epoxy resin and mixing it with superparamagnetic nanoparticles (see Methods). Using cyanoacrylate adhesive, we glued the magnetic resin to a resin block of embedded brain tissue, Fig. 1A.

To visualize the magnetic resin, we manually deposited a few ultrathin sections onto a pioloform grid and imaged them with a transmission EM, Fig. 1B. In high resolution EM imagery, the superparamagnetic particles appeared roughly uniformly distributed across the surface of the magnetic resin, Fig. 1C.

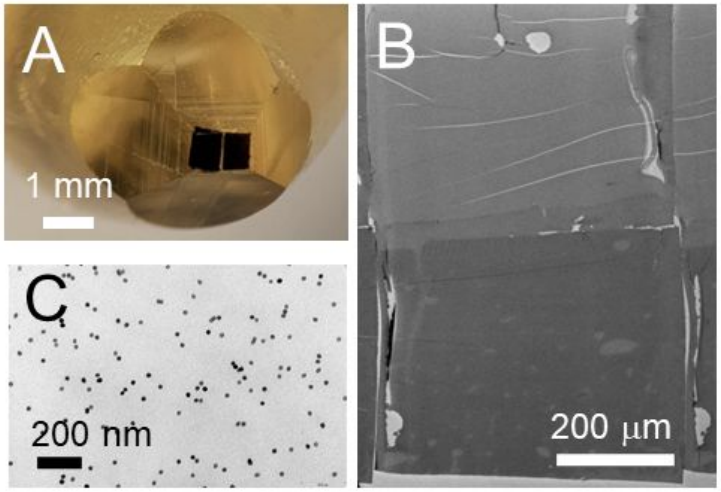

Figure 1. Magnetically augmented resin. *A) View of a magnetically augmented resin block, showing the parts containing superparamagnetic particles (black, left) and biological tissue (black, right). B) Electron transmission image of an ultrathin section, showing the tissue resin at the bottom and the magnetic resin at the top. C) Close-up EM image of the magnetic resin, showing superparamagnetic nanoparticles of circular shape.*

To collect the magnetic sections and place them onto a silicon wafer, we used a finely adjustable robotic arm that is easily assembled from a small set of inexpensive parts including a magnet, a 2-axis goniometer, and a 3-axis micromanipulator. To build the arm, the magnet is attached face-down to the goniometer and the latter is mounted on the micromanipulator via a thin extension made of aluminum.The assembled equipment for MagC is shown in Figure 2A.

After cutting several tens of sections of magnetically augmented tissue in a standard ultramicrotome with a large knife boat, the sections tended to disperse on the water surface, Fig. 2B. To collect the sections, we used the 3-axis manipulator and positioned the magnet at a distance of about 1 mm above the water surface. We adjusted the magnet's x-y position in the boat while keeping the distance to the water surface constant. We scanned the surface of the water with the magnet and returned the robotic arm to its initial position, upon which all sections were grouped without overlap near the center of the boat, Fig 2C.

Silicon wafers are ideal section collecting substrates thanks to their rigidity, flatness, chemical inertness, and conductivity. We deposited the sections onto wafers by draining the water from the boat using a syringe that we connected via a tube to a hole in the boat. While we drained the water with a syringe pump, we prevented the sections from

diffusing towards the walls of the boat by maintaining the magnet close to the water level. Using this procedure, it is possible to collect large numbers of sections at relatively high packing density.

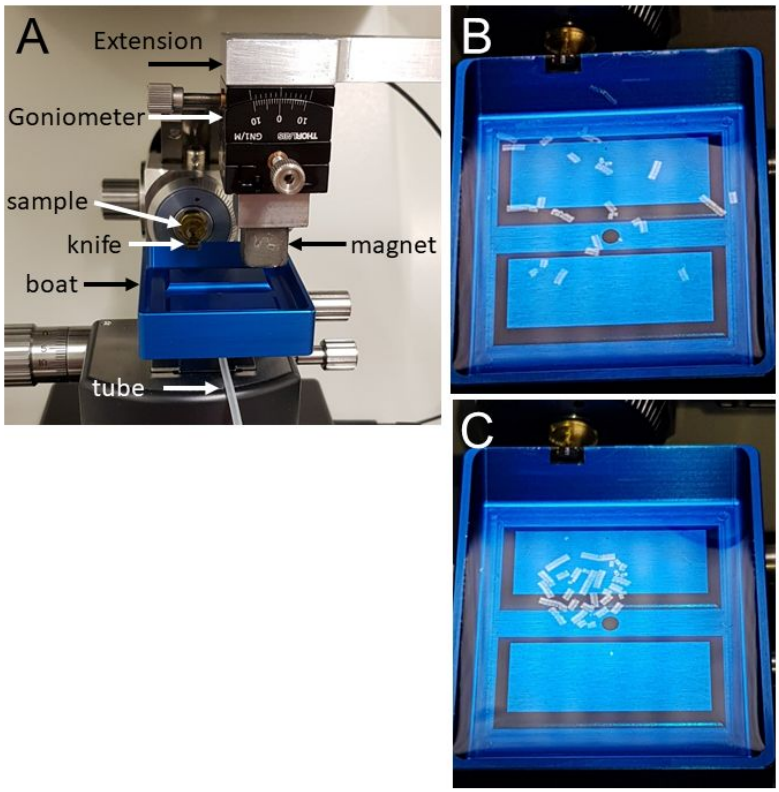

Figure 2. Magnetic section collection (MagC). *A) MagC setup. B) Free-floating magnetically augmented sections (gray) are dispersed on the water surface. C) After scanning the magnet across the sections 1 mm above the water surface, the sections are concentrated near the center of the boat.*

Given that the cutting order tends to get lost while ultrathin sections diffuse across the water surface, volumetric visualization requires digital restoration of the cutting order. Because consecutively cut sections are expected to be more similar in their appearance than sections far away on the block, the problem of finding the original cutting order can be addressed by computing the minimal path length in an open traveling salesman problem. The input to this problem is provided by the matrix of all pairwise section dissimilarities; the output is the estimated cutting order [6].

Fluorescence and electron microscopy

MagC is compatible with imaging techniques that make use of either light or electron microscopy, or both, such as correlative array tomography (CAT). As a CAT application of MagC, we processed brain samples in which diverse projection neurons had been fluorescently labeled using in-vivo injection of dextran-coupled retrograde tracers. In one adult male zebra finch, fluorescent tracers were injected into 3 distinct nuclei downstream of the song-control brain area HVC: Alexa Fluor 488 into RA, Fluorescein into Area X, and Texas Red in Avalanche, Fig. 3A. After magnetic augmentation, 512 ultrathin sections of 50 nm thickness were collected on a single silicon wafer [6].

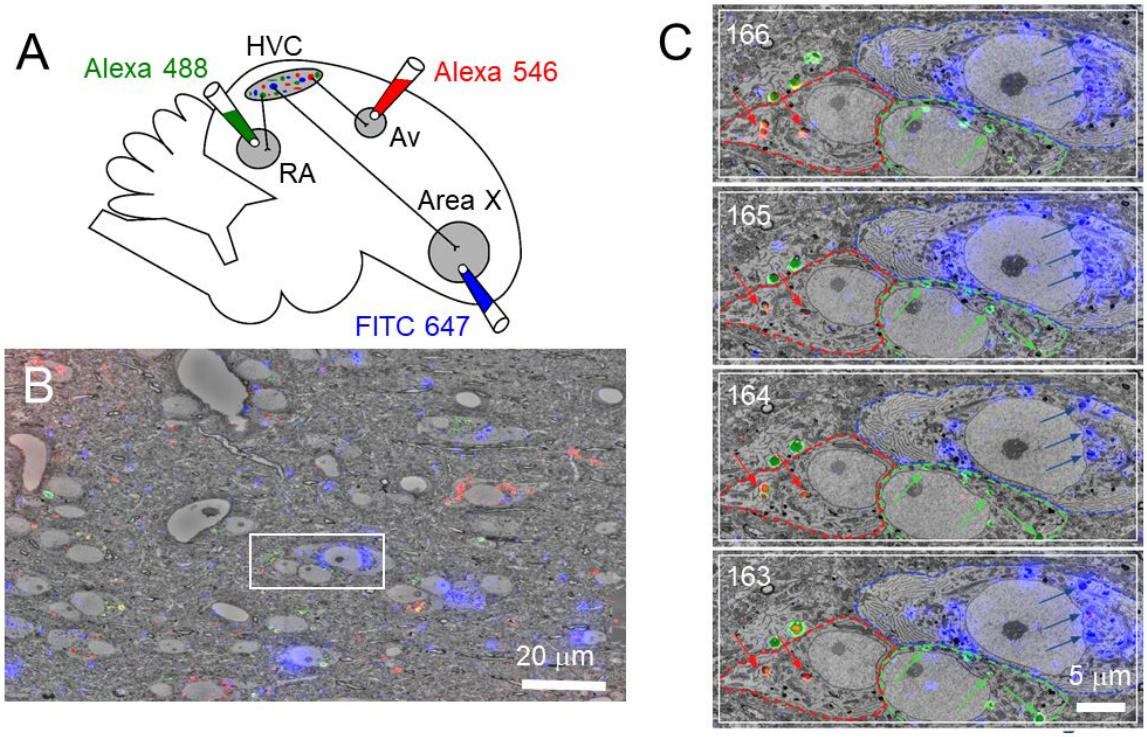

Figure 3. Suitability of MagC for correlative array tomography (CAT). *A) Schematic of the songbird brain. Fluorescent tracers were injected bilaterally in the robust nucleus of the arcopallium (RA, Alexa 488, green), Area X (FITC, blue), and Avalanche (Texas red, red). The tracers were retrogradely transported to label three neuron classes in HVC: HVC_{RA} neurons projecting to RA, HVC_{X} neurons projecting to Area X, and HVC_{Av} neurons projecting to Avalanche. B) Superposition of multi-color LM and EM imagery of a single ultrathin section. The white rectangle defines the image region shown in C. The LM imagery has been thresholded to highlight the localization of fluorescence in all three fluorescence channels. C) In four consecutive ultrathin sections (Sections 163-166), tracer signal is found mainly within lysosomes (colored arrows). Membranes*

of three neurons are delineated by dashed curves (blue: HVC_X, red: HVC_{Av}, green: HVC_{RA}).

To fix, stain, and embed brain tissue for EM tends to bleach fluorophores. Bleached fluorophores in ultrathin sections can be visualized using fluorescent antibodies against the fluorophores. After LM imaging of immunolabeled sections and subsequent EM imaging, the LM and EM imagery can be superimposed using a set of landmarks visible in both microscopes. As expected, based on previous work [15], the fluorescence labeling was most strongly expressed in lysosomes near the cell nucleus. Consistent labeling across at least 4 consecutive serial sections allows discrimination of three types of HVC projection neurons, Fig. 3C.

An important open question with regards to CAT applications for high-throughput neuroscience pertains to the feasibility of automated neuron identification. Visual inspection of consecutive sections does not scale well to very large volumes and very small neurites. As a first attempt to automatically identify the three expected projection neuron types in the CAT dataset shown in Fig. 3, we first randomly selected seven neurons in the EM imagery of the CAT dataset, Fig. 4A. We then semi-automatically segmented their somas (see Methods) and visually looked for somatic lysosomes with consistent coloring across at least 4 sections. We unambiguously identified 4/7 neurons as belonging to a known neuron type projecting either to Avalanche or RA, two neurons were double labelled (red/green and green/blue), and one neuron showed no consistent labeling within any somatic organelle, Fig. 4B. Using this visual inspection as gold standard, we evaluated a simple method of automatic neuron identification.

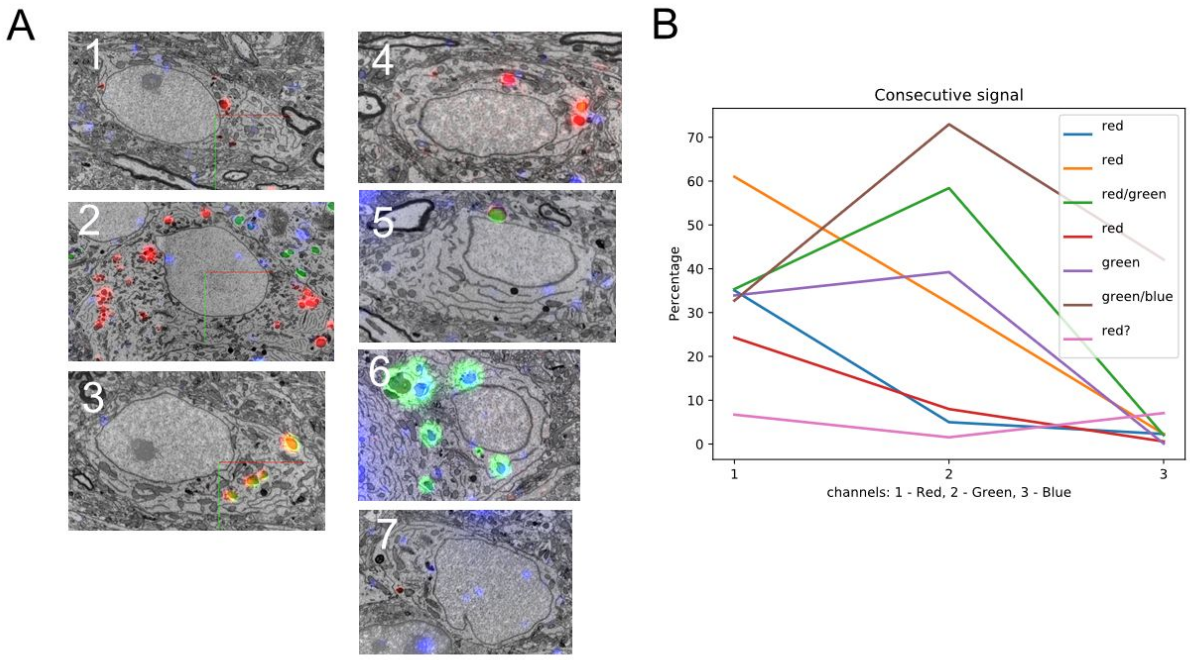

Figure 4. Two-section consistency as a measure to semi-automatically identify diverse types of projection neurons. *A) CAT snapshots of the soma of seven randomly selected neurons in the dataset. B) The percent consistently labeled pixels in consecutive sections shows that the peak percentage typically occurs in the channel (1=red, 2=gree, 3=blue) that has been visually identified as the determinant for neuron identification (legend).*

The automated method consisted of counting the percent supra-threshold pixels in the somatic region of a given section that were associated with a supra-threshold pixel in the following section at the exact same location. We term this co-localization measure *two-section consistency*. When plotting the two-section consistencies (as a percentage) for all 3 channels (red, green, and blue) and all seven neurons, we found decent agreement with the gold standard identification, Fig. 4A. Alone the double-labeled cells could not be unequivocally distinguished from single-labeled cells. However, the existence of doubly-projecting neurons remains an open issue and further animals will have to be examined to reach robust conclusions about such double projectors.

Conclusions

We independently verified the suitability of a histological method that provides a hands-free approach to high-resolution correlative light and electron microscopy. Compared to other systems for collecting hundreds of ultrathin sections such as ATUM,

MagC requires only a few components that can be easily fitted to standard commercial ultramicrotome systems. The ease with which we were able to collect the sections under the magnet, strengthens the conclusions drawn in [6].

For tissue reconstruction, homogeneous imagery of large tissue volumes is desirable. Homogeneity is promoted when the sectioning process is not interrupted, because interruptions can lead to section losses due to severe thickness variations. One way to prevent sectioning interruptions is to use a large knife boat. MagC is likely scalable to very large boats several tens of centimeters large. Alternatively, large volumes can be processed by cutting thick sections (on the order of hundreds of nanometers thick). To not compromise on imaging resolution, thick sections can be repeatedly imaged in a SEM and milled with broad ion beams [18].

So far, we have tested a roughly 1:1 ratio of embedded tissue to magnetic resin. By increasing the density of nanoparticles, it might be possible to achieve high section controllability also with much smaller amounts of magnetic resin, which could further increase the packing density of biological material on the imaging substrate. As a cautionary note, we observed that for excessively high density of superparamagnetic particles, particle agglomerates tend to form, which can hinder even cutting processes.

Currently, MagC requires the retrieval of the original cutting order by solving a traveling salesman problem. In future applications, it may be desirable to attempt to circumvent this post-processing step by keeping track of section order during cutting. Combined with super-resolution light microscopy techniques, MagC can provide a convenient building block for isotropic 3D reconstruction at the nanoscale.

To adopt MagC for routine CAT applications, we proposed a simple measure for neuron identification based on consecutive labeling consistency. We analysed in instance of two-section consistency and found promising agreement with visual identifications. We suspect that higher levels of section consistencies (across 3, 4, up to k sections) will provide even better results, provided ultrathin sections are thin enough to slice lysosomes at least k+1 times. We invite the computer vision community to further probe correlative neuron measures on our publicly released dataset.

Competing Interests

TT and RH hold a patent: Method, device, and system for manipulating portions of a rigid body, PCT/EP2016/078059 (Sep 2016).

Funding

RH acknowledges funding from: ETH Zurich Foundation (ETH Grant ETH-42 15-1) and ETH Equipment Grant 'Ultramicrotome, sample preparation device for microscopy' (2016).

Bibliography

1. Zewail, A. H. (2010). Four-dimensional electron microscopy. Science *328*, 187–193.
2. McMullan, G., Faruqi, A. R., and Henderson, R. (2016). Direct Electron Detectors. Meth. Enzymol. *579*, 1–17.
3. Schalek, R., Kasthuri, N., Hayworth, K., Berger, D., Tapia, J., Morgan, J., Turaga, S., Fagerholm, E., Seung, H., and Lichtman, J. (2011). Development of High-Throughput, High-Resolution 3D Reconstruction of Large-Volume Biological Tissue Using Automated Tape Collection Ultramicrotomy and Scanning Electron Microscopy. Microscopy and Microanalysis *17*, 966–967.
4. Micheva, K. D., and Smith, S. J. (2007). Array tomography: a new tool for imaging the molecular architecture and ultrastructure of neural circuits. Neuron *55*, 25–36.
5. Templier, T. (2019). MagC, magnetic collection of ultrathin sections for volumetric correlative light and electron microscopy. BioRxiv.
6. Templier, T., and Hahnloser, R. H. R. (2016). Automated dense collection of ultrathin sections directly onto silicon wafers. In Society for Neuroscience Meeting.
7. Oberti, D., Kirschmann, M. A., and Hahnloser, R. H. R. (2011). Projection neuron circuits resolved using correlative array tomography. Front. Neurosci. *5*, 50.
8. Burel, A., Lavault, M.-T., Chevalier, C., Gnaegi, H., Prigent, S., Mucciolo, A., Dutertre, S., Humbel, B. M., Guillaudeux, T., and Kolotuev, I. (2018). A targeted 3D EM and correlative microscopy method using SEM array tomography. Development *145*.
9. Cardona, A., Saalfeld, S., Schindelin, J., Arganda-Carreras, I., Preibisch, S., Longair, M., Tomancak, P., Hartenstein, V., and Douglas, R. J. (2012). TrakEM2 software for neural circuit reconstruction. PLoS ONE *7*, e38011.
10. Arganda-Carreras, I., Kaynig, V., Rueden, C., Eliceiri, K. W., Schindelin, J., Cardona, A., and Sebastian Seung, H. (2017). Trainable Weka Segmentation: a machine learning tool for microscopy pixel classification. Bioinformatics *33*, 2424–2426.
11. Preibisch, S., Saalfeld, S., and Tomancak, P. (2009). Globally optimal stitching of tiled 3D microscopic image acquisitions. Bioinformatics *25*, 1463–1465.

12. Schindelin, J., Arganda-Carreras, I., Frise, E., Kaynig, V., Longair, M., Pietzsch, T., Preibisch, S., Rueden, C., Saalfeld, S., Schmid, B., et al. (2012). Fiji: an open-source platform for biological-image analysis. Nat. Methods *9*, 676–682.

13. Lowe, D. G. (2004). Distinctive Image Features from Scale-Invariant Keypoints. Int. J. Comput. Vis. *60*, 91–110.

14. Cook, W. Concorde TSP Solver. Available at: http://www.math.uwaterloo.ca/tsp/concorde.html [Accessed December 20, 2018].

15. Oberti (2010). Correlative microscopy of densely labeled projection neurons using neural tracers. Front. Neuroanat.

16. Neurodataviz Available at: http://neurodata.io [Accessed December 20, 2018].

17. Neuroglancer Available at: http://github.com/google/neuroglancer [Accessed December 20, 2018].

18. Langford, R. M., and Petford-Long, A. K. (2001). Broad ion beam milling of focused ion beam prepared transmission electron microscopy cross sections for high resolution electron microscopy. J. Vac. Sci. Technol. A *19*, 982–985.